Front. Earth Sci. 2018, 12(2): 373–380
https://doi.org/10.1007/s11707-017-0664-x

RESEARCH ARTICLE

# On the classification of mixed floating pollutants on the Yellow Sea of China by using a quad-polarized SAR image

**Xiaochen WANG[1,2], Yun SHAO[1], Wei TIAN (✉)[1,3], Kun LI[1]**

1 Institute of Remote Sensing and Digital Earth, Chinese Academy of Sciences, Beijing 100101, China
2 University of Chinese Academy of Sciences, Beijing 100049, China
3 Joint Institute for Regional Earth System Science and Engineering and Department of Atmospheric and Oceanic Sciences, University of California, Los Angeles, CA 90095, USA



**Abstract** This study explored different methodologies using a C-band RADARSAT-2 quad-polarized Synthetic Aperture Radar (SAR) image located over China's Yellow Sea to investigate polarization decomposition parameters for identifying mixed floating pollutants from a complex ocean background. It was found that solitary polarization decomposition did not meet the demand for detecting and classifying multiple floating pollutants, even after applying a polarized SAR image. Furthermore, considering that Yamaguchi decomposition is sensitive to vegetation and the algal variety *Enteromorpha prolifera,* while H/A/alpha decomposition is sensitive to oil spills, a combination of parameters which was deduced from these two decompositions was proposed for marine environmental monitoring of mixed floating sea surface pollutants. A combination of volume scattering, surface scattering, and scattering entropy was the best indicator for classifying mixed floating pollutants from a complex ocean background. The Kappa coefficients for *Enteromorpha prolifera* and oil spills were 0.7514 and 0.8470, respectively, evidence that the composite polarized parameters based on quad-polarized SAR imagery proposed in this research is an effective monitoring method for complex marine pollution.

**Keywords** RADARSAT-2, polarization decomposition, mixed floating pollutants, classification

## 1 Introduction

In the past decade, the frequency of marine environmental accidents, such as oil spills and large-scale macroalgae blooms (MABs), has resulted in the deterioration of oceanic ecosystems and threats to maritime safety (Fletcher, 1996; Hu et al., 2010). *In-situ* marine disaster investigations by ship and plane are not always practical due to severe weather conditions or difficult to reach offshore zones where such disasters often occur. Therefore, sea surface monitoring day and night is an important asset. Among the variety of remote sensing technologies that are available, Synthetic Aperture Radar (SAR) is able to operate in all weather conditions and is unaffected by clouds and precipitation. Oil spills and *Enteromorpha prolifera* are interpreted as surface disaster features on the sea surface in SAR imagery (Brekke and Solberg, 2005; Zhang et al., 2011; Solberg, 2012). The detection and classification of mixed floating pollutants from a complex ocean background still remain to be investigated with respect to the application of SAR remote sensing for the marine environment (Liu et al., 2013; Nunziata et al., 2014).

In the application of single-polarized SAR imagery for classification of typical surface disaster features, gray features, texture, geometry, and other features can be extracted (Hu, 2009; Wang et al., 2009; Liu et al., 2010). However, only the ocean surface backscattering coefficient is related to the physical mechanisms of mixed floating pollutants, which is not sufficient enough to investigate their characteristics from a complex ocean background or to facilitate their detection and classification.

With the advent of dual-polarized and quad-polarized technology, more polarization information is now available that could be potentially more useful than the conventional single-polarized SAR mode. In the study of quad-polarized SAR images for the classification of typical floating pollutants on the sea surface, Migliaccio et al. (2009b) found that the H/alpha density histogram could be used to

Received December 31, 2016; accepted April 23, 2017

E-mail: tianwei@radi.ac.cn

efficiently classify different types of oil spills. He also demonstrated that, of the three typical polarization parameters, polarization entropy was the best factor for oil spills detection in regions with high wind speeds. Meanwhile, Migliaccio et al.'s oil spills experiment (Migliaccio et al., 2007) concluded that the circular polarization correlation (CPC) and polarization anisotropy were sufficient for oil spill detection using the L and C bands from SIRC/X SAR data. In addition, Migliaccio et al. (2009a) demonstrated the effectiveness of ALOS PALSAR polarized SAR images in the detection of oil spills on the sea surface. Wang (Liu et al., 2011) proposed combining three polarization feature decomposition parameters and the co-polarized correlation coefficient and found that it could be effectively applied to detect oil spills on the sea surface. Meanwhile, Tian et al. (2010) investigated the discrimination between different kinds of crude oil and their look-alikes using RADARSAT-2 SAR images over the South China Sea, as well as the potential for using polarized SAR imagery for oil spills classification. Shirvany et al. (2012) concluded that the degree of polarization had high application potential in sea oil spills detection. Minchew et al. (2012) analyzed L-band quad-polarized UAV SAR data during the Gulf of Mexico oil spill and found that single scattering dominated on the oily surface at incident angles of 26° and −60°. He also concluded that the main eigenvalue of the polarization scattering matrix was the most reliable factor for oil spill detection. Wang et al. (2010) collated multi-temporal SAR images with buoy data on currents and wind products retrieved from the SeaWinds scatterometer, and they further forecasted the *Enteromorpha prolifera* drift trend analysis. Kudryavtsev et al. (2013) demonstrated the utility of combining co-polarized SAR data with polarization differences, polarization ratios, and non-polarized components for classifying different sea surface features such as waves, currents, oil spills, and wind.

Until now, many studies have investigated typical floating pollutants detection, but few studies have focused on the classification of mixed floating pollutants from a complex ocean background. Because different floating pollutants may be similar in their intensity, it can be difficult to directly classify mixed floating pollutants from quad-polarized SAR imagery. In order to improve classification of mixed floating pollutants from a complex ocean background, we introduce a polarization target decomposition theory for quad-polarized SAR imagery data processing.

In this study, we used a RADARSAT-2 quad-polarized SAR image collected in 2016 over China's Yellow Sea to classify mixed floating pollutants, such as oil spills, *Enteromorpha prolifera*, and vegetation. In Section 2, we briefly introduce the study area and dataset selected for this study. Different polarization decomposition methods are demonstrated and applied for data processing in Section 3. In Section 4, polarization parameters extracted using different decomposition methods are compared and further analyzed. Finally, an optimum combination of polarization parameters is proposed. Conclusions are provided in Section 5.

## 2 Study area and data

### 2.1 Study area

The study area is located in the Yellow Sea of China, with respective longitude and latitude of 32°30′–36°30′N and 109°00′–123°30′E. The Yellow Sea is a semi-closed sea that connects the Eurasian continent and the Pacific Ocean. It has important economic and political significance for numerous countries in Asia, but in the past decade, its environmental quality has been in decline. In addition to some oil pollution resulting from occasional leaks in crude oil shipping and petroleum exploitation, annual large-scale blooms of *Enteromorpha prolifera* algae usually occur in the middle of the Yellow Sea during May or June (Shi and Wang, 2009; Liu et al., 2015), which drift to the offshore areas of Shandong province due to wind and sea currents, resulting in severe threats to ocean ecosystems and maritime safety (Zhang et al., 2013; Yoshida et al., 2015).

### 2.2 Dataset

In this study, a C-band RADARSAT-2 quad-polarized SAR image of the Yellow Sea of China was analyzed. Detailed information for the image is listed in Table 1.

Figure 1 shows the pseudo-color composite image, which was captured in July of 2016 during a time when vegetation fully covers Laoshan Mountain (in the upper left corner of Fig. 1). This is also the time of year when *Enteromorpha prolifera* blooms, shown in Zone 2, occur in the Yellow Sea off the eastern coast of Qingdao. An oil spill was identified by RADARSAT-2, as shown in Zone 3. In addition to these features, vegetation and open water, corresponding to Zones 1 and 4, respectively, were also confirmed by an on-site survey carried out to verify the scope and presence of the MABs that occurred in the Yellow Sea during summer 2016.

The SAR composite image therefore provides an opportunity to investigate the detection and classification of typical marine objects, which were simultaneously

**Table 1** Specifications of the C-band RADARSAT-2 quad-polarized SAR image

| Location | Time (UTC) | Acquisition mode | Incidence angle | Pass | Beam | Resolution |
|---|---|---|---|---|---|---|
| The Yellow Sea of China | 2016-7-4 22:07 | Fine Quad-pol | 25.8°–27.6° | Descend | FQ 7 | 5 m |

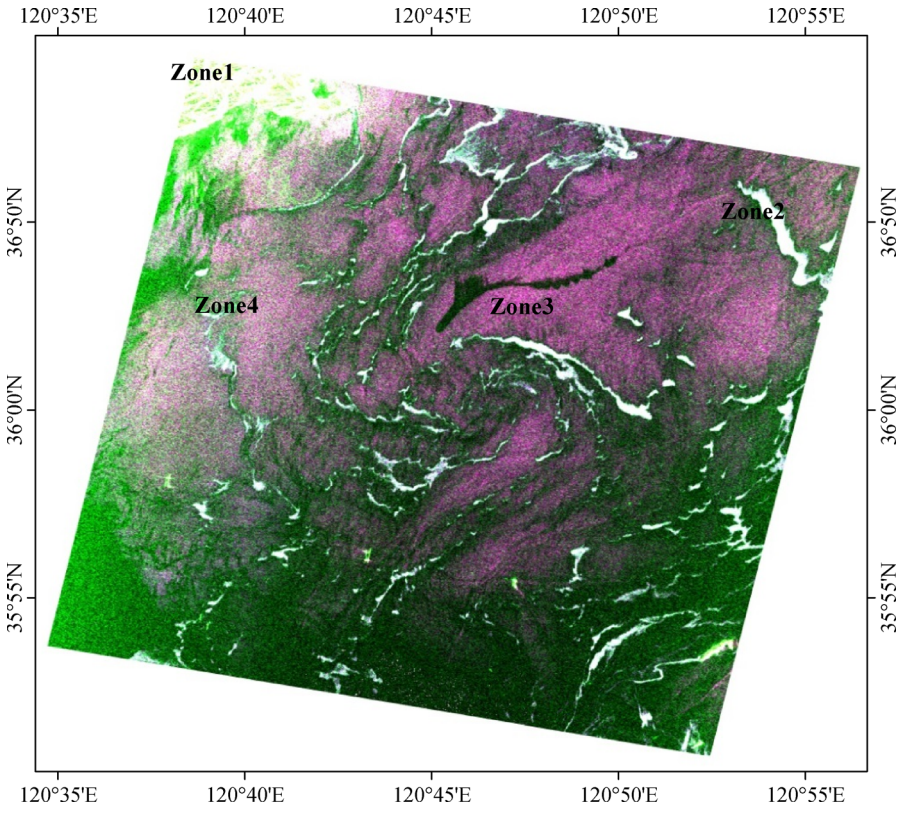


**Fig. 1** C-band RADARSAT-2 quad-polarized SAR image (R: HH G: HV B: VV). The image time (UTC) was 22:07 on 7/4/2016, the swath was 25 km×25 km, the resolution was 5.2 m×7.6 m, and Zones 1 to 4 correspond to vegetation, *Enteromorpha prolifera*, oil spills, and open water, respectively.

collected by the quad-polarized SAR sensor, so that the uncertainty and unreliability of the classification algorithm can be significantly reduced. In this study, we used this image for further classification of mixed floating pollutants, which can be seen as typical marine features in SAR imagery.

## 3 Methods and data processing

In this section, we introduce the polarization target decomposition method to classify mixed floating pollutants by decomposing the target scattering matrix into the superposition of a simple scattering formula. We also discuss which decomposition components can be used to describe the structural and physical features of typical sea surface objects. Finally, different decomposition methods are performed to process and analyze the data.

### 3.1 Polarization decomposition

#### 3.1.1 Freeman-Durden decomposition

Freeman and Durden decomposed the covariance matrix into the sum of surface scattering, double bounce scattering, and volume scattering (Freeman and Durden, 1998). Among these, surface scattering derived from first-order Bragg scattering was used to describe a moderately rough surface, double bounce scattering derived from the orthogonal plane of different dielectric constants was used to describe dihedral corner reflection, and volume scattering derived from random oriented dipole was used to describe cloud canopy. This verifies the fact that Freeman-Durden decomposition can be used to accurately describe the scattering of natural objects.

#### 3.1.2 Yamaguchi decomposition

Freeman-Durden decomposition is based on the assumption of reflection symmetry theory, which is illustrated by the following formula: $\langle S_{HH}S_{HV}^{*}\rangle = \langle S_{HV}S_{VV}^{*}\rangle = 0$. But in certain complex regions, the reflection symmetry condition can no longer be satisfied. In order to extend the applicability of Freeman-Durden decomposition, Yamaguchi introduced the additional items $\langle S_{HH}S_{HV}^{*}\rangle \neq 0$ and $\langle S_{HV}S_{VV}^{*}\rangle \neq 0$ to describe the reflection asymmetry condition (Yamaguchi et al., 2006, 2011; Sato et al., 2012). They also proposed the four-elements target decomposition method. In Yamaguchi decomposition, the helix scattering mechanism was expressed as a left-handed or

right-handed circular polarized state of scattering, which can be used to describe the complexity of artificial targets. In addition to helix scattering, Yamaguchi modified the volume scattering component by varying the relative azimuthal probability density function, while Freeman used a dipole model with a random azimuth to describe the volume scattering term (Yamaguchi et al., 2005).

#### 3.1.3 H/A/alpha decomposition

Cloud proposed a new decomposition method based on entropy theory. Unlike the previous polarization decomposition methods, they defined scattering entropy and scattering angle to describe the changes from homogeneously random scattering to completely random scattering, and average scattering from surface scattering to double bounce scattering, respectively (Cloude and Pottier, 1996). They also defined the concept of anisotrophy to analyze the relationship between these two weak scattering components (Cloude and Pottier, 1997).

### 3.2 Data processing

SSC data from RADARSAT-2 quad-polarized SAR imagery was pre-processed using the PolSARpro platform.

The covariance matrix (C3) was extracted from SSC data from a C-band RADARSAT-2 quad-polarized SAR image prior to any processing. The C3 was processed as an input parameter for further polarization decomposition. Here we chose three classical polarization decomposition methods: Freeman-Durden decomposition, Yamaguchi decomposition and H/A/alpha decomposition. The extraction window was set to size = 10 to extract the decomposition components using these methods. Additional data processing steps were also performed, including multi-look processing, de-noising, and projection transformation. The final results of each respective polarization decomposition method are shown in Figs. 2–4.

### 3.3 Statistical analysis

The Freeman-Durden decomposition components are shown in Figs. 2(a)–2(c), which correspond to surface scattering, double bounce scattering, and volume scattering, respectively. For vegetation cover, volume scattering dominated among all three components. There was very little partial double bounce scattering or surface scattering in the decomposition results. For open water, surface scattering dominated among all the scattering types with little double bounce scattering or volume scattering. On the other hand, *Enteromorpha prolifera* exhibited strong surface scattering and volume scattering but weaker double bounce scattering, while all three scattering components for oil spills were weak compared to the other land cover types.

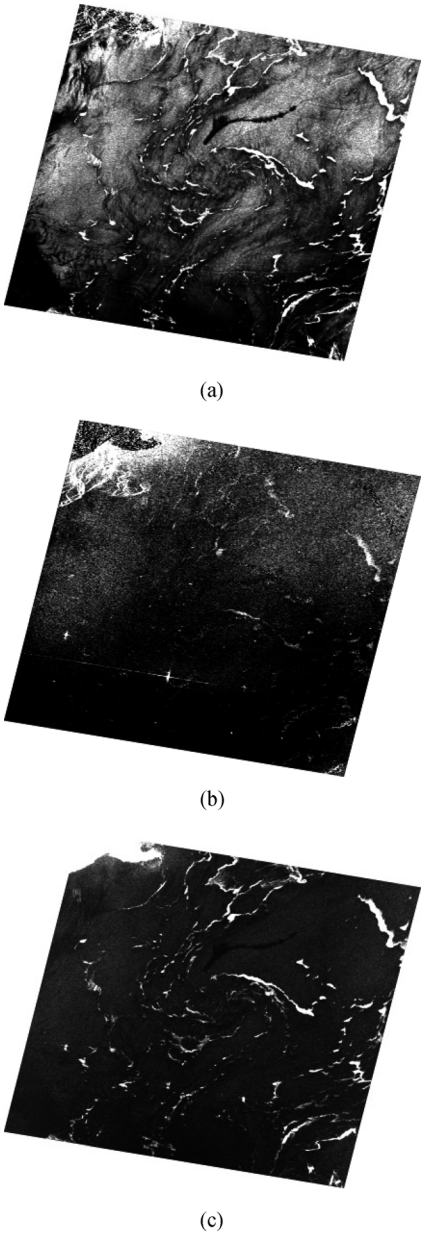

(a)

(b)

(c)

**Fig. 2** Different scattering components for vegetation, open water, *Enteromorpha prolifera*, and oil spills following Freeman-Durden decomposition: (a) surface scattering; (b) double bounce scattering; (c) volume scattering.

The Yamaguchi decomposition components are shown in Figs. 3(a)–3(d), which correspond to surface scattering, double bounce scattering, volume scattering, and helix scattering, respectively. The vegetation component in the Yamaguchi decomposition (Fig. 3) shared some characteristics with the Freeman-Durden decomposition (Fig. 2). However, open water had weaker volume scattering components, which contrasted with the Freeman-Durden decomposition results. In fact, the Bragg scattering mechanism is typically used to describe open water because there is basically no volume scattering on the

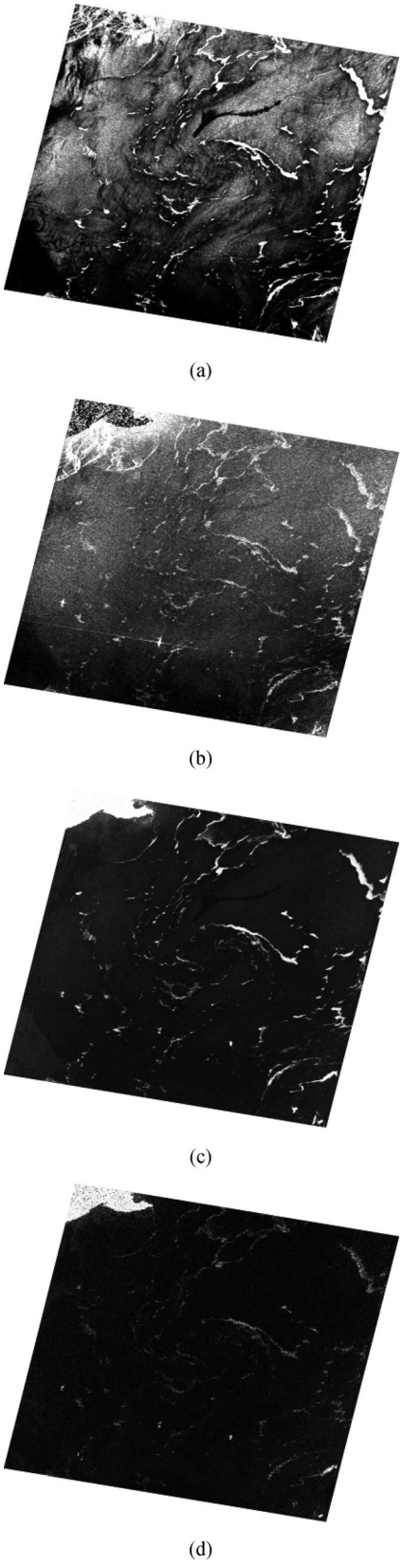

(a) (b) (c) (d)

**Fig. 3** Different scattering components for vegetation, open water, *Enteromorpha prolifera*, and oil spills following Yamaguchi decomposition: (a) surface scattering; (b) double bounce scattering; (c) volume scattering; (d) helix scattering.

ocean surface, so one can conclude that Freeman-Durden is not suitable for open water. Additionally, vegetation and *Enteromorpha prolifera* had strong helix scattering, but those components for open water and oil spills were approximately zero. There was also partial double bounce scattering in the *Enteromorpha prolifera* decomposition component, especially near shore, which is a subject for future research.

The H/A/alpha decomposition components are shown in Figs. 4(a)–4(c), which correspond to scattering entropy, scattering angle, and scattering anisotropy, respectively.

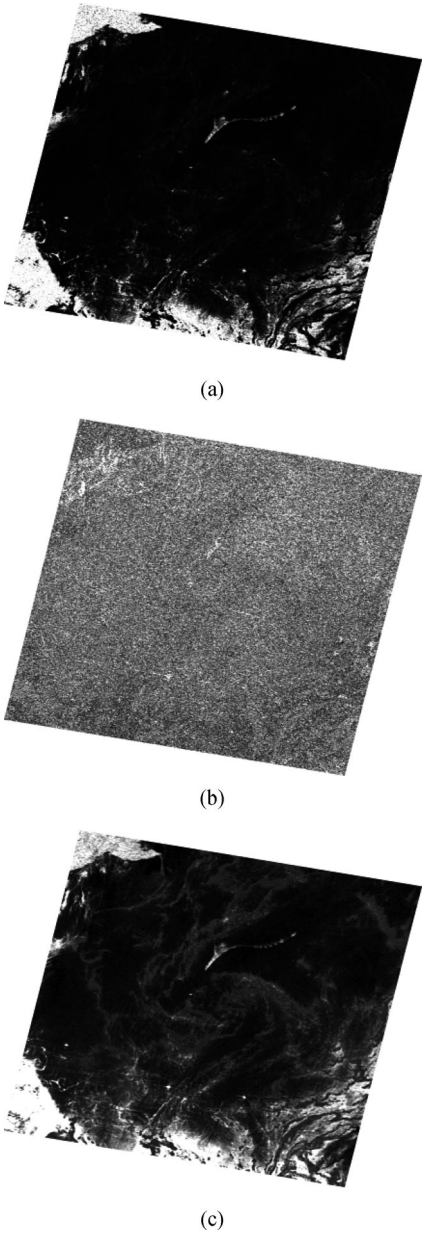

(a) (b) (c)

**Fig. 4** Different scattering components for vegetation, open water, *Enteromorpha prolifera*, and oil spills following H/A/alpha decomposition: (a) scattering entropy; (b) scattering angle; (c) scattering anisotropy.

Vegetation and oil spills had high scattering entropy, while *Enteromorpha prolifera* and open water had very low scattering entropy in H/A/alpha decomposition (Fig. 4). All targets had a similar scattering angle. On the other hand, *Enteromorpha prolifera* had weaker scattering anisotropy than vegetation and oil spills, but was slightly higher than that of open water.

## 4 Results and discussion

To more accurately evaluate the polarization decomposition components, a select number of pixels representing vegetation, open water, *Enteromorpha prolifera*, and oil spills were extracted using different decomposition methods. Some polarization parameters were also calculated and analyzed as shown in Table 2. To evaluate the decomposition components, we used Michelson's contrast criteria (Shurcliff, 1963) to describe the between-region contrast, which can be expressed by:

$$C = \frac{F_{\max} - F_{\min}}{F_{\max} + F_{\min}}, \quad (1)$$

where $F_{\max}$ and $F_{\min}$ are the maximum and minimum image values, respectively. The larger the value of $C$, the better identification ability of polarization parameter has.

After comparing the different target polarization parameters in Table 2, we concluded that the different floating pollutants had contrasting behaviors based on the polarization parameters, so this sensitivity of polarization parameters can be used to improve pollutant classification.

The surface scattering and double bounce scattering in the Freeman-Durden decomposition were similar to those from the Yamaguchi decomposition; however, the volume scattering term in the Freeman-Durden decomposition was overestimated, which contradicts the actual sea surface conditions. Therefore, we selected the Yamaguchi decomposition results for further analysis. The double bounce scattering for *Enteromorpha prolifera* was approximate 0.002 and for vegetation it was 0.006, while both open water and oil spills had approximately zero values based on the Yamaguchi decomposition. The surface scattering results for *Enteromorpha prolifera* and vegetation were similar, about 0.12, which was higher than open water and oil spills. The volume scattering result for vegetation was 0.18, higher than that of *Enteromorpha prolifera* at 0.004. Apart from vegetation, the helix scattering for the remaining targets was almost zero. Clearly, we can identify vegetation and *Enteromorpha prolifera* using the Yamaguchi decomposition. However, oil spills still cannot be distinguished from the oceanic background.

In order to classify open water and oil spills, the H/A/alpha decomposition was also applied during data processing. We found that vegetation had the largest scattering entropy value of about 0.48, while open water had the smallest scattering entropy value of about 0.005. Moreover, the scattering entropy of *Enteromorpha prolifera* and oil spills had moderate values of 0.01 and 0.06, respectively, with the oil spills registering slightly higher than *Enteromorpha prolifera*. Therefore, open water and oil spills can be distinguished based on their scattering entropy. In addition, the scattering anisotropy values of the four target types were relatively similar, around 0.4. The scattering angle for vegetation had the largest value of about 38.1, and the values of the scattering angles were very similar for open water, *Enteromorpha prolifera*, and oil spills, at 7.3, 11.9, and 13.1, respectively.

Based on the above analysis, we found that no single parameter could be used to fully describe the contrast between mixed floating pollutants, so we proposed an optimum combination of polarization parameters based on the three polarization decomposition methods for mixed floating pollutants classification. For better comparison, according to the ratio of each target in any polarization scattering component, we used high, moderate, and low to describe the relative magnitude of decomposition polarization parameters. The results are shown in Table 3.

In order to quantitatively evaluate the accuracy of combining polarization parameters for mixed floating

**Table 2** Polarization parameters for floating pollutants under different polarization decomposition methods

| Method | Parameter | Vegetation | Open water | *Enteromorpha prolifera* | Oil spills | *C* |
|---|---|---|---|---|---|---|
| Freeman-Durden decomposition | Dbl | 0.0041 | 0.00064 | 0.00083 | 0.00057 | 0.7558 |
| | Odd | 0.0662 | 0.0572 | 0.1214 | 0.0287 | 0.6175 |
| | Vol | 0.2809 | 0.0018 | 0.0076 | 0.0012 | 0.9914 |
| Yamaguchi decomposition | Dbl | 0.0065 | 0.00081 | 0.0016 | 0.00066 | 0.8156 |
| | Odd | 0.0646 | 0.0576 | 0.1232 | 0.029 | 0.6189 |
| | Vol | 0.1802 | 0.00092 | 0.0037 | 0.00061 | 0.9932 |
| | Hlx | 0.0472 | 0.00013 | 0.00074 | 0.00011 | 0.9953 |
| H/A/alpha decomposition | H | 0.478 | 0.0052 | 0.01 | 0.0594 | 0.9896 |
| | A | 0.4247 | 0.4632 | 0.4623 | 0.4827 | 0.0639 |
| | alpha | 38.14 | 7.3467 | 11.918 | 13.1388 | 0.6769 |

**Table 3** The optimum polarization parameters combination for mixed floating pollutants classification

| Paremeter | Vegetation | Open water | *Enteromorpha prolifera* | Oil spills |
|---|---|---|---|---|
| Odd | Moderate | Moderate | High | Low |
| Vol | High | Low | Moderate | Low |
| H | High | Low | Low | High |

**Table 4** The typical targets classification accuracy for optimum decomposition parameters

| Parameter | Vegetation | Open water | *Enteromorpha prolifera* | Oil spills | Kappa |
|---|---|---|---|---|---|
| Odd | 0.114 | 0.057 | 0.028 | 0.123 | 0.6935 |
| Vol | 0.278 | 0.0008 | 0.0156 | 0.0004 | 0.6233 |
| H | 0.530 | 0.007 | 0.079 | 0.187 | 0.6533 |
| Composite | | | | | 0.9555 |

pollutants classification, we used a maximum likelihood method. We selected 160,000 pixels for each polarization parameter, 80,000 of which were used to train the classification and the remaining 80,000 were used for evaluation. The optimum polarization parameters combination statistics and Kappa coefficient for each floating pollutant are shown in Table 4, and the pseudo composite image of the optimum polarization parameters is also shown in Fig. 5.

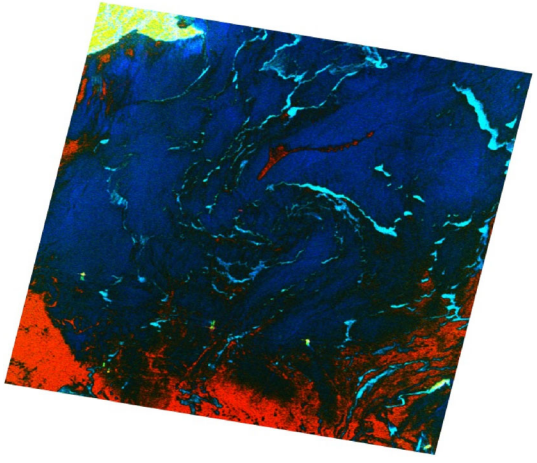

**Fig. 5** A pseudo composite image of the optimum polarization parameters.

## 5 Conclusions

This study used a C-band RADARSAT-2 quad-polarization SAR image over China's Yellow Sea to analyze and discuss the applicability of different polarization decomposition methods for the detection and classification of mixed floating pollutants on the sea surface. This study also compared and analyzed the sensitivity of polarization parameters to different floating pollutants. Based on the polarization parameter sensitivity, an optimum combination for pollutant classification was also proposed. The main conclusions of this paper are as follows.

Freeman-Durden decomposition is not suitable for the classification of sea surface targets because the volume scattering component is overestimated when compared with Yamaguchi decomposition results. It was found that results from the Yamaguchi decomposition were more precise than Freeman-Durden decomposition in terms of discriminating between typical targets on the sea surface.

The polarization parameters derived from any single polarization decomposition method cannot meet the demands for detecting and classifying mixed floating pollutants. The Yamaguchi decomposition method can be used for recognizing vegetation and *Enteromorpha prolifera*, while H/A/alpha can be used for recognizing oil spills.

The optimum combination of polarization parameters for the detection and classification of mixed floating pollutants on the sea surface was volume scattering and scattering entropy. The sensitivity of this parameter combination could be summarized as follows: vegetation had high values for both polarization parameters; open water had low values for both; *Enteromorpha prolifera* had moderate volume scattering values but low scattering entropy values; and oil spills had low volume scattering values with high scattering entropy values.

**Acknowledgements** The authors gratefully acknowledge financial support from the National Natural Science Foundation of China (Grant Nos. 41301500, 41431174, and 61471358). This paper was partly sponsored by a Funding of Scholarship from the Chinese Academy of Sciences. The authors would also like to acknowledge on-site teamwork by Dr. Juan Wang et al. of the North China Sea Environmental Monitoring Center, State Oceanic Administration.

## References

Brekke C, Solberg A H S (2005). Oil spill detection by satellite remote sensing. Remote Sens Environ, 95(1): 1–13

Cloude S R, Pottier E (1996). A review of target decomposition theorems in radar polarimetry. IEEE Trans Geosci Remote Sens, 34(2): 498–518

Cloude S R, Pottier E (1997). An entropy based classification scheme for land applications of polarimetric SAR. IEEE Trans Geosci Remote Sens, 35(1): 68–78

Fletcher R L (1996). The occurrence of "green tides"— A reivew. In: Schramm W, Nienhuis P H, eds. Marine Benthic Vegetation. Springer Berlin Heidelberg, 7–43

Freeman A, Durden S L (1998). A three-component scattering model for polarimetric SAR data. IEEE Trans Geosci Remote Sens, 36(3): 963–973

Hu C M (2009). A novel ocean color index to detect floating algae in the global oceans. Remote Sens Environ, 113(10): 2118–2129

Hu C, Li D, Chen C, Ge J, Muller-Karger F E, Liu J, Yu F, He M X (2010). On the recurrent *Ulva prolifera* blooms in the Yellow Sea and East China Sea. J Geophys Res, 115(C5): C05017

Kudryavtsev V N, Chapron B, Myasoedov A G, Collard F, Johannessen J A (2013). On dual co-polarized SAR measurements of the ocean surface. IEEE Geosci Remote Sens Lett, 10(4): 761–765

Liu D, Keesing J K, He P, Wang Z, Shi Y, Wang Y (2013). The world's largest macroalgal bloom in the Yellow Sea, China: formation and implications. Estuarine Coastal & Shelfence, 129: 2–10

Liu P, Li X, Qu J J, Wang W, Zhao C, Pichel W (2011). Oil spill detection with fully polarimetric UAVSAR data. Mar Pollut Bull, 62 (12): 2611–2618

Liu P, Zhao C, Li X, He M, Pichel W (2010). Identification of ocean oil spills in SAR imagery based on fuzzy logic algorithm. Int J Remote Sens, 31(17–18): 4819–4833

Liu X, Li Y, Wang Z, Zhang Q, Cai X (2015). Cruise observation of *Ulva prolifera* bloom in the southern Yellow Sea, China. Estuar Coast Shelf Sci, 163: 17–22

Migliaccio M, Gambardella A, Nunziata F, Shimada M, Isoguchi O (2009a). The PALSAR polarimetric mode for sea oil slick observation. IEEE Transactions on Geoscience & Remote Sensing, 47(12): 4032–4041

Migliaccio M, Gambardella A, Tranfaglia M (2007). SAR polarimetry to observe oil spills. IEEE Trans Geosci Remote Sens, 45(2): 506–511

Migliaccio M, Nunziata F, Gambardella A (2009b). On the co-polarized phase difference for oil spill observation. Int J Remote Sens, 30(6): 1587–1602

Minchew B, Jones C E, Holt B (2012). Polarimetric analysis of backscatter from the deepwater horizon oil spill using L-band synthetic aperture radar. IEEE Trans Geosci Remote Sens, 50(10): 3812–3830

Nunziata F, Migliaccio M, Li X (2014). Sea oil slick observation using hybrid-polarity SAR architecture. IEEE Journal of Oceanic Engineering, 1(2): 426–440

Sato A, Yamaguchi Y, Singh G, Park S E (2012). Four-component scattering power decomposition with extended volume scattering model. IEEE Geosci Remote Sens Lett, 9(2): 166–170

Shi W, Wang M (2009). Green macroalgae blooms in the Yellow Sea during the spring and summer of 2008. J Geophys Res, D, Atmospheres, 114(C12): C12010

Shirvany R, Chabert M, Tourneret J Y (2012). Ship and oil-spill detection using the degree of polarization in linear and hybrid/compact dual-pol SAR. IEEE Journal of Selected Topics in Applied Earth Observations & Remote Sensing, 5(3): 885–892

Shurcliff W (1963). Studies in optics. Journal of Physics and Chemistry of Solids, 24(3): 498–499

Solberg A H S (2012). Remote sensing of ocean oil-spill pollution. Proc IEEE, 100(10): 2931–2945

Tian W, Shao Y, Yuan J, Wang S, Liu Y (2010). An Experiment for Oil Spill Recognition Using RADARSAT-2 Image. IEEE International Geoscience & Remote Sensing Symposium, IGRASS 2010, 2761–2764

Wang S, Zhang F, Shao Y, Tian W, Gong H (2010). Microwave Remote Sensing for Marine Monitoring: An Example of *Enteromorpha prolifera* Bloom Monitoring. IEEE International Geoscience & Remote Sensing Symposium, IGRASS 2010, 4530–4533

Wang X H, Li L, Bao X, Zhao L D (2009). Economic cost of an algae bloom cleanup in China's 2008 Olympic sailing venue. Eos (Wash DC), 90(28): 238–239

Yamaguchi Y, Moriyama T, Ishido M, Yamada H (2005). Four-component scattering model for polarimetric SAR image decomposition. IEEE Trans Geosci Remote Sens, 43(8): 1699–1706

Yamaguchi Y, Sato A, Boerner W M, Sato R, Yamada H (2011). Four-component scattering power decomposition with rotation of coherency matrix. IEEE Transactions on Geoscience & Remote Sensing, 49(6): 2251–2258

Yamaguchi Y, Yajima Y, Yamada H (2006). A four-component decomposition of POLSAR images based on the coherency matrix. IEEE Geosci Remote Sens Lett, 3(3): 292–296

Yoshida G, Uchimura M, Hiraoka M (2015). Persistent occurrence of floating *Ulva* green tide in Hiroshima Bay, Japan: seasonal succession and growth patterns of *Ulva pertusa* and *Ulva* spp. (Chlorophyta, Ulvales). Hydrobiologia, 758(1): 223–233

Zhang B, Perrie W, Li X, Pichel W G (2011). Mapping sea surface oil slicks using RADARSAT-2 quad-polarization SAR image. Geophys Res Lett, 38: L10602

Zhang J H, Huo Y Z, Zhang Z L, Yu K F, He Q, Zhang L H, Yang L L, Xu R, He P M (2013). Variations of morphology and photosynthetic performances of *Ulva prolifera* during the whole green tide blooming process in the Yellow Sea. Mar Environ Res, 92(6): 35–42